applied sciences

MDPI

Article

An Off-Body Narrowband and Ultra-Wide Band Channel Model for Body Area Networks in a Ferryboat Environment

Krzysztof K. Cwalina *, Slawomir J. Ambroziak and Piotr Rajchowski

Faculty of Electronics, Telecommunications and Informatics, Gdansk University of Technology, 80-233 Gdańsk, Poland; slawomir.ambroziak@pg.edu.pl (S.J.A.); piorajch@eti.pg.edu.pl (P.R.)
* Correspondence: kkcwalina@eti.pg.edu.pl

Received: 23 April 2018; Accepted: 14 June 2018; Published: 16 June 2018

Abstract: In the article an off-body narrowband and ultra-wide band channel model for body area networks in a ferryboat environment is described. Considering the limited number of publications there is a need to develop an off-body channel model, which will facilitate the design of radio links, both from the multimedia services provider and the security point of view, for body area networks in this atypical environment. A mobile heterogeneous measurement stand, using radio distance measurements, which consists of three types of devices: miniaturized mobile nodes, stationary reference nodes, and a data acquisition server, was developed. A detailed analysis of both radio channels' parameters was carried out. An analysis of system loss for off-body communication, including mean system loss, large-scale fading (corresponding to body shadowing), and small-scale fading (associated with the multipath phenomenon), both for 868 MHz narrowband and for 6489 MHz ultra-wide band channels, was performed. A statistical analysis of the obtained system loss model parameters was also carried out; good fit to the empirical data is observed.

Keywords: wireless body area networks; off-body communication; ferryboat environment; narrowband; ultra-wide band; system loss; path loss; system loss model

1. Introduction

The development of mobile radio communication systems is related to constantly growing expectations and the needs of the users. The first generation of mobile telephony (1G) was launched in 1979 and was based on analog transmission. At the beginning of the 1990s, there was a significant breakthrough in the standardization of the mobile telephony. The implementation of the second-generation (2G) Global System for Mobile Communications (GSM) network offered not only voice services, but also transfer of data, text, and multimedia messages, indicated a milestone in the technological progress. Then, at the turn of the 21st century, the Universal Mobile Telecommunications System (UMTS) system was introduced, which is the third-generation (3G) mobile telephony standard. Almost a decade later, miniaturization of electronic devices and technological progress in terms of increase in computational power, as well as growing expectations for various services offered by service providers, initiated the development of the Long-Term Evolution (LTE) and LTE Advanced systems, which are recognized as the fourth-generation system (4G). A fast growth of data transmission and spectral efficiency, as well as the reduced delays of point-to-point transmission in the whole network, are some of the main goals achieved during the implementation of this system [1–3].

The trend of introducing the next generations of systems every decade can be seen, so it is expected to launch the first fifth-generation (5G) systems around 2020. It is supposed to be a significant technological leap in relation to existing systems, not only due to a significant increase in the data rate

(reaching 10 Gbps), network reliability, and energy efficiency of devices, and reduced transmission delays (less than 1 ms), but also the introduction of new frequency bands, multi-antenna techniques, and the development of a completely new architecture. The emergence of the Internet of Things (IoT) concept, i.e., gathering and data exchange between smart devices, has resulted in a rapid increase in radio communications between such devices installed in homes, in cars, on the streets, or even on and inside the human body. In particular, devices working within the human body, e.g., monitoring life parameters, performing localization services, or providing media services, have become more important.

According to the data from analytical companies [4], in 2016 the number of wearable devices increased much faster than the number of smartphones, and in the next years the disproportion will become significant due to the exponential growth in the number of the former. This means that the device used as a mobile phone is no longer the main telemetry device, and it will actually become a controller of peripheral devices located around it. This type of a radio network, consisting of peripheral devices operating within the human body, is called a wireless body area network (WBANs), defined also as a body area network (BANs).

The problems associated with this kind of network are known from previous-generation systems, or even wireless sensor networks (WSNs), and include, among others, energy consumption, quality of service (QoS), transmission techniques, dynamic frequency band management, and radio channel modelling in various propagation environments. However, one should remember that, in WBANs, the body (human or animal) itself has a crucial impact on the radio link, as well as its motion, and the placement of wearable or implantable nodes [2,5–10].

The rest of the paper is structured as follows: In Section 2, the current state of the art is briefly presented. Section 3 describes the used measurement stand. In Section 4, measurement scenarios are characterized. Section 5 contains an analysis of the model components, while the final model statistical analysis is provided in Section 6. The article is concluded in Section 7.

2. Related Work

The rapid technological progress in development of small size wearable devices dedicated for WBANs does not eliminate the key problem of ensuring a stable radio link. In these types of networks one has to deal with high system losses, i.e., introduced by the human body and multipath propagation in the environment, especially for applications with dynamic users. The indoor propagation issues, concerning WBANs, are widely analyzed by researchers. The majority of currently designed WBANs are used in indoor environments in which radio wave propagation is significantly disturbed compared to open space, mainly due to the stronger multipath effect. In the current state of the art, many indoor off-body channel models were proposed, but still there is a need to perform additional measurements and analytical studies for other types of environments. Therefore, it was decided to carry out measurements in a passenger ferryboat, which is an atypical and very harsh environment in terms of a radio wave propagation. Due to its metal structure, it cannot be treated as a typical indoor environment.

The obtained measurements allowed for development of an off-body channel model, which will facilitate the design of WBANs. It is very important, both from the perspective of multimedia service providers, as well as the security point of view. The practical example of WBAN operating in the ferryboat is a system for remote tracking and monitoring of people, developed at the Department of Radio Communication Systems and Networks, Gdansk University of Technology [11]. This system was developed for the Polish Maritime Regional Unit of Border Guard, and its goal was to increase the security of the officers on duty. It consists of off-body personal identification modules, which are mounted directly on the human body, while reference nodes are attached to the ferryboat's construction elements. The telemetry data about the officers are sent to the operating center.

Several previous research studies in this environment analyzed ultra-wide band (UWB) channels operating in the 6–9 GHz band and narrowband (NB) channels operating in the 2.4 GHz band. In [12], measurements of NB 2.4 GHz radio channel in a similar ferryboat environment were carried out.

Despite the environments' similarities, the main goal of the analysis was to evaluate a simple model for stationary surveillance network. In [13], measurements were carried out for an on-body UWB channel. The proposed model consists of a normally distributed random variable, which represents the received signal variations due to fading. The work in [14] is focused on obtaining a statistical model for the UWB propagation channel in a ferryboat passenger cabin. Moreover, the measurements were focused on determining and further modeling of the channel impulse response, not the system loss. In [15], the developed path loss model was evaluated for UWB off-body communication, where the fading is modeled by a Gaussian variable, but the model was not investigated in the ferryboat environment. The most complex model for WBANs in a ferryboat is proposed in [16]. It accounts for the mean system loss (MSL), and attenuation due to fading. The measurement scenarios were dynamic, but only the NB channel at 2.45 GHz is analyzed.

Considering the limited number of publications related to channel modeling in the passenger ferryboat and the growing interest in the use of WBANs in such an environment, the conducted research and proposed novel system loss model is unique. It should also be noted that the authors have used custom measurement equipment, which uses radio distance measurements (RDMs) to dynamically estimate the distance between the moving person and the static reference node (RN). This approach gives accurate data despite the different user motion velocities during the measurements.

3. Measurement Equipment

Conducting measurements of NB and UWB in the real environment required the development of heterogeneous nodes adapted to work around the human body. The proposed measurement equipment consists of three types of devices: mobile node (MN), stationary R,N and data acquisition server (DAS).

The MN and the RN have similar hardware design. The only difference, from the electrical diagram point of view, is the existence of the RS-232 wired interface in RN. In Figure 1, a block diagram of the MN is presented.

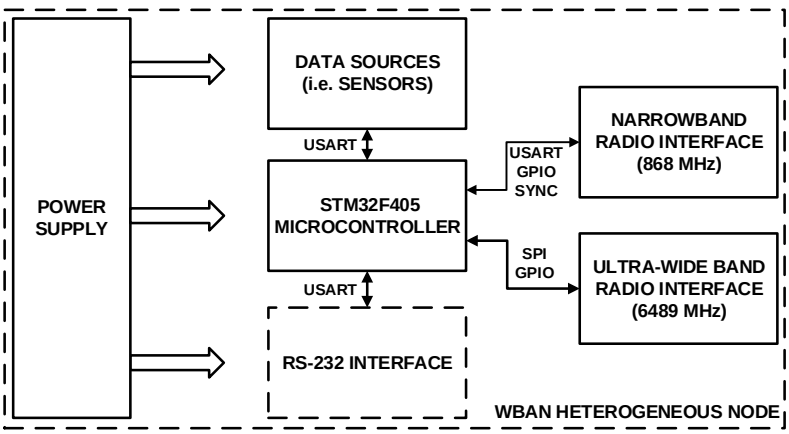

Figure 1. A block diagram of the MN.

Each MN and RN is heterogeneous, in the sense that it has two simultaneously working, time synchronized radio interfaces:

- NB radio module CC1120 from Texas Instruments, working in the ultra-high frequency (UHF) 868 MHz band [17],
- UWB radio module DWM1000 from DecaWave, working in the super-high frequency (SHF) 6489 MHz band [18].

Both radio interfaces work in accordance with the IEEE 802.15.4 standard, including the operating frequencies in the Wireless Medical Telemetry Service (WMTS) and UWB bands for Europe, which is indicated as possible for use in WBANs [19].

The selected parameters of the 868 MHz module should be mentioned: center frequency 868.3 MHz, 5 dBm of output power, 2-GFSK (Gaussian frequency shift keying) modulation with frequency deviation of 50 kHz, 50 kbps bitrate, 67 B packet data length with data whitening included. The antenna for the NB interface is Yageo's compact ceramic antenna ANT1204F007R0870A [20], with 1.67 dBi gain, resonance frequency equal to 870 MHz, and reflection loss −28 dB. The choice of antenna was motivated by its physical dimension and the possibility of using it in miniaturized devices.

The selected UWB parameters for the measurements are as follows: 6489 MHz center frequency, −41.3 dBm/MHz transmitted power spectral density and 499.2 MHz of the occupied bandwidth. The ACS5200HFAUWB ceramic omnidirectional antenna element for the UWB interface is integrated in the DW1000 module [21].

The DAS includes a GETAC F110 industrial tablet [22], together with a dedicated DAS server application. The custom developed dedicated software is a multi-threaded application, which allows for continuous monitoring of the obtained telemetry data and the status of each network node.

4. Measurement Scenarios

Propagation measurements were conducted on the passenger ferryboat, named Motor Ferry WAWEL (MF WAWEL), during mooring at the port quay. During the measurements, only the crew was present on the ferryboat. Structural elements of the environment (i.e., walls, ceiling, floor, doors, and handrails) are made of steel of various thicknesses.

For all considered scenarios, the stationary RN was attached to the corridor wall at a height of 1.2 m, on the seventh passenger deck. A single MN was placed on the user moving along the axis of a narrow corridor. The separation between human skin and radiating elements was about 1 cm. The measurements were carried out by one user: a man with a height of 1.72 m, a weight of 60 kg and a body mass index (BMI) of 20.3.

In Figure 2, a schematic diagram of the measurement equipment is shown. It illustrates the places where MN were mounted. From many possible mounting locations, three were selected as representative for WBANs applications, including smart watches, heart rate monitors, multimedia glasses, etc. [7,23,24]. These are:

- right side of the head (HE_R), with the height of h_{HE} = 1.65 m;
- chest (TO_F), with the height of h_{TO} = 1.35 m; and
- left wrist (AB_L), with the height of h_{AB} = 0.9 m.

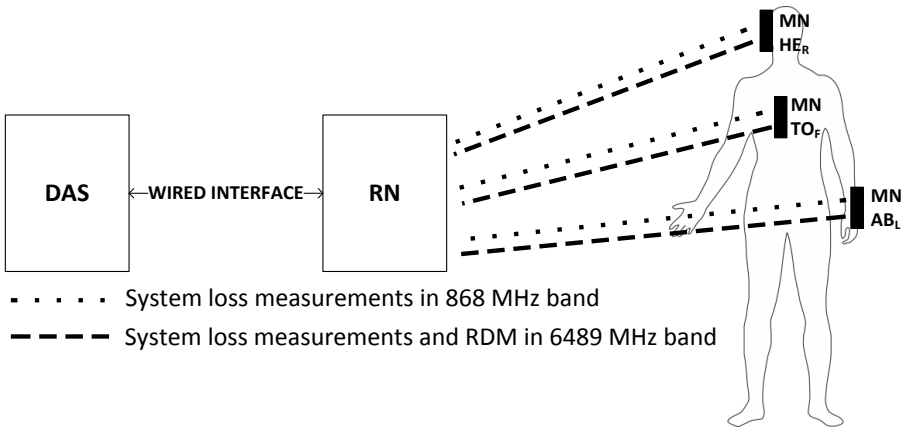

Figure 2. A schematic diagram of the measurement equipment.

Typically, in other works [23–25], the distance between measurement points was calculated on the basis of the average speed of the user. This required continuous supervision during the measurements

and manual determination of the beginning and the end of the measurement data recording process. During the presented research, RDM were performed by using the Symmetrical Double-Sided Two-Way Ranging (SDS-TWR) measurement method [26]. This allowed for the full automation of the system loss measurements. Time synchronization of both radio interfaces, using a dedicated signal line, allowed for obtaining the information on the system loss value and the corresponding distance between the receiver (Tx) and the receiver (Rx) at a given moment. Thus, all measurement data were recorded and analyzed regardless of the speed of the user in different phases of the scenario.

It is known that static scenarios are characterized by a smaller spread of propagation attenuation around the mean value and a smaller error in distance estimation using RDMs due to the absence of the small-scale fading component associated with the user's body motion, or lack of changes of its position. For this reason, it was decided to analyze only dynamic scenarios, which are much more complex in terms of radio wave propagation [25,27,28].

The measurements were carried out for two dynamic scenarios (SCNs): approaching to (APR), and departing from (DEP), the RN. These two scenarios correspond to a typical human behavior in indoor environments, and they are widely considered in WBAN research. They allow for the analysis of the measurement data independently of the side of the body on which the node is located, i.e., regardless of the antenna's placement on the left or right wrist. For the DEP scenario, the user started the motion at the distance of 2 m from the RN with the line-of-sight (LOS) conditions and walked towards the end point through the L-shaped corridor. After 6.5 m along the walking path there is a change between the zone with LOS conditions and the zone behind the corridor's corner with non-LOS (NLOS) conditions. The walk ended after travelling a distance of 14 m. In Figure 3, a floor plan of the investigated environment, which is a part of the passenger ferryboat's seventh deck, is shown.

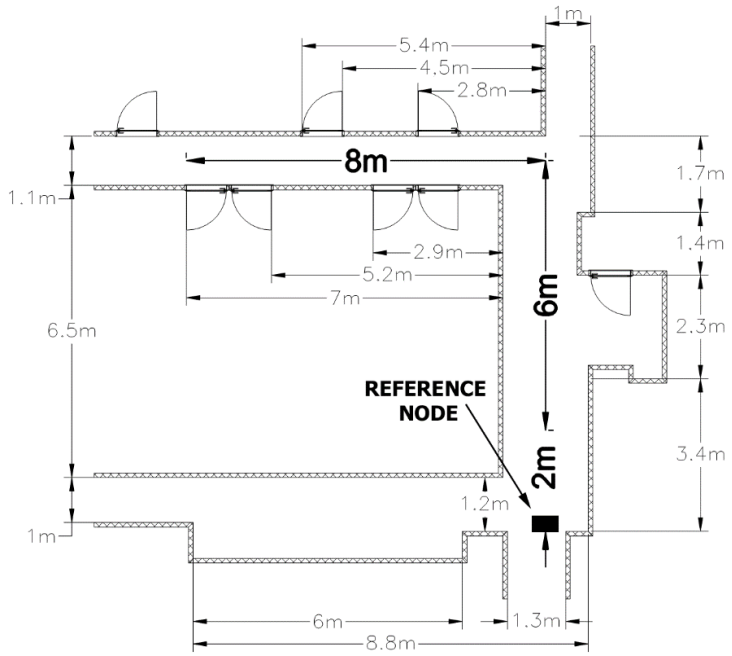

Figure 3. A plan of the investigated scenario—part of the passenger ferryboat's seventh deck.

The LOS and NLOS conditions were determined by the presence of the metallic walls between MN and RN. The APR scenario is reversed with respect to the DEP one, i.e., from the aspect of the walking direction and the starting and ending points of the route. For each scenario and MN placement, the measurements were repeated 20 times. During the measurements, there were no other people in the corridor nor inside the passenger cabins.

5. Analysis of the Results

During the measurements, 87,252 system loss values were collected with 40 ms interval between the consecutive measurements, for NB and UWB, for both motion scenarios and all three MN placements. It should be mentioned that the preliminary results, including the mean and the standard deviation system loss values are presented in [29,30], hence, they are not analyzed in detail in this article. The corresponding RDM were collected simultaneously. It should be pointed out that, in this article, the propagation attenuation is understood as the system loss [31], i.e., the difference in power delivered to the transmitting antenna and the power available at the terminals of the receiving one.

The preliminary analysis of the empirical system loss values for both frequency bands showed that the propagation model should include the estimation of the system loss separately for LOS and NLOS conditions, and separately for each MN placement. The results of the distance estimation by RDM indicated the significant differences in the radio wave propagation across the environment. In this environment the waves propagate along the corridor due to the metal structure and the waveguide effect, unlike in the typical indoor environments, where the radio waves can propagate along the direct line (even through the walls) between MN and RN [29,30].

The system loss ($L_{SL(\mathrm{dB})}$) is modeled by the general following expression:

$$L_{SL(\mathrm{dB})} = \overline{L_{S(\mathrm{dB})}} + \Delta L_{BS(\mathrm{dB})} + \Delta L_{MF(\mathrm{dB})}, \quad (1)$$

where:

- $\overline{L_S}$ is the MSL component,
- ΔL_{BS} is the body shadowing component represented by a random variable, and
- ΔL_{MF} is the multipath component represented by a random variable.

5.1. Mean System Loss Component

The MSL component represents the decrease in the received signal power with distance due to absorption and dissipation of energy in the propagation medium, which is represented as follows:

$$\overline{L_{S(\mathrm{dB})}} = \overline{L_S(d_0)_{(\mathrm{dB})}} + 10 \cdot n \cdot \log_{10}\left(\frac{d_{[\mathrm{m}]}}{d_{0[\mathrm{m}]}}\right), \quad (2)$$

where:

- $\overline{L_S(d_0)}$ is MSL value at the reference distance d_0 (d_0 = 2 m for LOS and d_0 = 8 m for NLOS),
- n is system loss exponent (SLE), and
- d is the distance between Tx and Rx.

The MSL component was obtained by fitting the logarithmic distance function to the empirical data. Linear regression with the least squares method was used.

To analyze the accuracy of linear model, two well know measures were used, namely standard error of estimate (SEE), representing the standard deviation of empirical data around the regression line, and mean error (ME) [32].

The obtained values of the SLE (n) and the MSL ($\overline{L_S(d_0)}$) at reference distance d_0, both for 868 MHz and 6489 MHz bands, are presented in Table 1.

There are visible differences between the MSL parameters for various scenarios, placements of MN, and for different radio interfaces (NB and UWB). For each scenario, a significant differences in both parameters for the LOS and NLOS conditions were observed. The ME error was 0 dB, which means that the MSL model parameters are correctly estimated from the measurements.

In the 868 MHz NB channel the multipath propagation phenomenon and the waveguide effect in the corridor are clearly visible. The values of n for LOS conditions are in the range of [0.16; 0.34], being

below the free-space value of 2 [33]. For NLOS, excluding the HE_R scenario, the parameter n is in the range of [1.40; 3.80]. These differences are related to the high power level of the multipath components reaching the antenna compared to the power of the direct component [34]. The noticeably low value for the HE_R scenario (0.16) can be explained by the unique environmental conditions, in which there is a strong reflected component from the opposite side of the corridor wall. Moreover, the polarizations of both antennas were matched and their mutual orientation changed to a small extent. As expected, the MSL at the reference distance is greater under NLOS conditions for most cases, but these differences are not significant. The SEE does not exceed the value of 3 dB for all the scenarios.

Table 1. Obtained values of SLE and MSL at reference distance.

MN LOCATION	SCENARIO	LOS/NLOS Conditions	NB		UWB	
			n	$\overline{L_S(d_0)}_{(\mathrm{dB})}$	n	$\overline{L_S(d_0)}_{(\mathrm{dB})}$
HE_R	APR	LOS	0.32	75.9	0.61	23.4
		NLOS	2.56	72.1	3.46	26.1
	DEP	LOS	0.34	71.9	0.79	25.7
		NLOS	0.16	76.2	3.12	27.7
TO_F	APR	LOS	0.24	64.7	0.13	24.0
		NLOS	2.51	65.9	2.41	27.3
	DEP	LOS	0.34	73.3	0.85	28.4
		NLOS	1.40	73.6	2.16	29.5
AB_L	APR	LOS	0.16	68.3	0.54	25.6
		NLOS	3.80	69.7	1.25	30.7
	DEP	LOS	0.21	70.8	0.27	28.9
		NLOS	2.95	71.9	2.58	28.4

Similar to the NB channel, there are also differences between the MSL model parameters for the UWB channel. The results show a significant difference in between the values of n for the LOS and NLOS conditions. Similar conclusions based on empirical data are presented in the available literature [14,35,36]. For the LOS conditions, the n values are in the range of [0.13; 0.85]. As expected, these values are below the free-space value, which is caused by the waveguide effect. It was also noticed that, similar to the NB interface, the highest value of n (0.85) was obtained for the DEP scenario and the TO_F placement. However, the obtained values of n for the NLOS conditions are in the range of [1.25; 3.46]. The two highest values of n were obtained for the MN mounted on the head (HE_R). Almost all scenarios are characterized by a higher MSL at the reference distance for the NLOS conditions relative to the LOS ones; the difference never exceeds 5.1 dB. The obtained SEE does not exceed the value of 3.1 dB.

5.2. Body Shadowing Component

According to Equation (1), one of the key elements of the system loss is represented by the component associated with the body shadowing ΔL_{BS}. Due to the random nature of human motion, ΔL_{BS} is also random, thus, it is represented by a random variable.

Obtaining the ΔL_{BS} component is possible by a low-pass filtration of the empirical data. The method of this filtration depends on the analyzed measurement scenario. In static scenarios, the empirical data are averaged over time, yielding the composite component $\overline{L_{SL}(d)}$, i.e.:

$$\overline{L_{SL}(d)} = \overline{L_S(d)} + \Delta L_{BS} = \frac{1}{N_t}\sum_{i=0}^{N_t} L_{SL}(d,i), \tag{3}$$

where N_t is the number of received signal samples obtained within a certain time window for the analyzed distance.

In dynamic scenarios, the filtration of the empirical data cannot be performed directly by using Equation (3) and requires spatial filtering due to the variable distance between the measurement nodes. Such filtration was realized with a linear moving average filter, which can be described by the following expression:

$$\overline{L_{SL}(d)} = \frac{1}{M} \sum_{j=0}^{M-1} L_{SL}[k-j],\ k = M,\ M+1,\ M+2, \ldots N_t, \tag{4}$$

where M is the length of the averaging window, which includes the number of samples corresponding to ten wavelengths (10λ). This is the selected value of the spatial filter resolution, determined from measurements [27]. It should be mentioned that the user's motion velocity was varying during the measurements, thus, the length of the filter was adjusted. These factors determined the development of the adaptive filter, whose length is selected on the basis of the estimated parameters of the user's motion during the measurements.

The body shadowing component is obtained by subtracting the MSL (Equation (2)) from the composite component (4), i.e.:

$$\Delta L_{BS} = \overline{L_{SL}(d)} - \overline{L_S(d)}. \tag{5}$$

In order to model the large-scale fading component, the best fitting probability distribution was chosen. Due to the physics of the underlying phenomena, the losses affecting the received signal add up in the logarithmic domain. This yields a lognormal distribution of the large-scale fading component, as confirmed by the numerous studies available in the literature [37].

The lognormal probability distribution was fitted to the empirical data in linear domain (ΔL_{BS}). This was done in MATLAB, using the *fitdist* function, which is the implementation of the maximum likelihood estimation.

In Figure 4, some examples of the lognormal probability density functions (PDFs) fitted to the empirical fading distribution for one of the measurement scenarios in NB channel were presented. The goodness-of-fit (GoF) metrics, i.e., the correlation coefficient (r) and the chi-square (χ^2) test were also evaluated. The correlation coefficient should be higher than the adopted acceptability threshold $r_{TH} = 0.90$. The threshold value for the chi-square test, i.e., for the significance level $\alpha = 0.05$, is $\chi^2_{th} = 28.87$ for Rayleigh distribution, and $\chi^2_{th} = 27.58$ for the others.

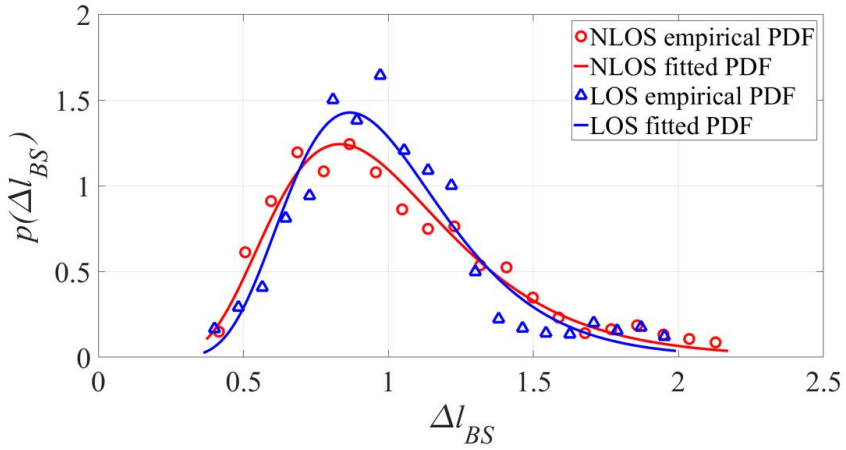

Figure 4. Exemplary results of the lognormal probability density functions fitted to empirical large-scale fading distributions (for DEP, HE_R, NB).

In order to visualize the obtained results in the best way, it was decided to present the distribution parameters, i.e., the average value μ and standard deviation σ in the logarithmic scale. In Table 2, the parameters of the fitted lognormal distribution are shown. The average value oscillates around

0 dB, which is in line with the results presented in the literature [28,29]. It also means that the adaptive low-pass filter (Equation (4)) was correctly implemented.

Table 2. The parameters of lognormal PDF fitted to the empirical large-scale fading distributions.

868 MHz NB Channel						
MN LOCATION	**SCENARIO**	**LOS/NLOS Conditions**	**μ (dB)**	**σ (dB)**	**χ^2**	**r**
HE_R	APR	LOS	−0.3	1.8	8.91	0.84
		NLOS	−0.4	2.7	13.4	0.92
	DEP	LOS	−0.2	1.3	2.94	0.96
		NLOS	−0.2	1.6	6.92	0.98
TO_F	APR	LOS	−0.1	0.8	0.78	0.37
		NLOS	−0.2	1.9	15.4	0.70
	DEP	LOS	−0.3	2.0	7.01	0.96
		NLOS	−0.2	1.6	7.04	0.89
AB_L	APR	LOS	−0.2	1.2	0.34	0.96
		NLOS	−0.3	1.9	6.92	0.99
	DEP	LOS	−0.3	1.8	7.35	0.97
		NLOS	−0.2	1.5	4.59	0.97
6489 MHz UWB Channel						
MN LOCATION	**SCENARIO**	**LOS/NLOS Conditions**	**μ (dB)**	**σ (dB)**	**χ^2**	**r**
HE_R	APR	LOS	−0.2	1.2	3.74	0.98
		NLOS	−0.2	1.8	8.97	0.99
	DEP	LOS	−0.3	2.1	18.88	0.96
		NLOS	−0.3	2.2	17.59	0.91
TO_F	APR	LOS	−0.2	1.3	5.20	0.67
		NLOS	−0.2	1.7	10.74	0.74
	DEP	LOS	−0.2	1.7	4.79	0.94
		NLOS	−0.3	2.6	40.34	0.97
AB_L	APR	LOS	−0.3	2.2	10.11	0.94
		NLOS	−0.3	2.8	21.84	0.99
	DEP	LOS	−0.3	2.1	12.26	0.95
		NLOS	−0.3	2.8	20.34	0.94

For the NB channel the standard deviation is in the range of [1.2; 2.7] for almost all scenarios; the lower limit was obtained for LOS and the upper one for NLOS conditions. This range is wider than it is presented in the literature [28], i.e., [1.49; 1.52]. This is caused, among others factors, by the waveguide effect, which yields to a greater spread of the results for various MN placements.

All fitted distributions have passed the chi-square test. The value of the correlation coefficient in most cases is greater than the acceptance threshold. Only for the APR scenario and the MN placement on the chest (TO_F) can a significantly low (0.37) r parameter be observed. Therefore, this scenario was not taken into account during the analysis of the standard deviation.

For the UWB channel the observed standard deviation values are in the range of [1.3; 2.8], similarly as for the NB channel; the lower values were obtained for the LOS, while the higher ones were obtained for the NLOS conditions. In the majority of the analyzed scenarios, the standard deviation is higher for the UWB channel. Although both NB and UWB bands are significantly different in terms of frequency, occupied bandwidth, resistance to multipath effects, and frequency selectivity, it can be noticed that the values of the standard deviations are proportional to each other only if the differences between particular scenarios are considered.

The average value of σ equals 1.7 dB for NB and 2 dB for UWB channel. The obtained results show that the lognormal distribution, in general, properly represents the shadow fading component regardless of the MN placement and the propagation conditions.

5.3. Multipath Component

The system loss model for off-body communication (Equation (1)) also takes the small-scale fading component ΔL_{MF} into account. It represents the impact of the user's motion and the multipath effect. Due to the random nature of this phenomenon, ΔL_{MF} also has a random character and is represented by a random variable.

Extraction of ΔL_{MF} is possible by subtracting the value of the composite component $\overline{L_{SL}(d)}$ (Equation (4)) from instantaneous values of the system loss L_{SL}, i.e.:

$$\Delta L_{MF(\mathrm{dB})} = L_{SL(\mathrm{dB})} - \overline{L_{SL}(d)_{(\mathrm{dB})}} \tag{6}$$

The methodology of determining the empirical distribution of the small-scale fading component and fitting the theoretical PDFs is very similar to that used for the body shadowing component, ΔL_{BS}, and is also performed in the linear domain (ΔL_{MF}).

Based on the literature dealing with the small-scale fading distributions, both for NB and UWB channels, the most frequently used ones were selected for fitting, i.e., lognormal, Rice, Rayleigh, Weibull, and Nakagami-*m*. For WBAN channels, the lognormal, Weibull, and Nakagami-*m* distributions were indicated as those that most accurately represent the small-scale fading amplitude distribution. Statistically, Rice and Rayleigh distributions are less often used for these channels [38].

In Figure 5, the exemplary results of the selected PDFs fitted to the empirical distribution of multipath fading is shown. Rice- and Rayleigh-fitted PDFs' distribution parameters were similar. This may be caused by the fact that, in a strong multipath environment like the investigated one, there is no dominant direct component, and the received signal is a sum of a large number of reflected components. Apparent asymmetry of the empirical distribution around the mean value makes the lognormal distribution the best fitting one. Apart from the subjective assessment, the GoF test has been performed using the correlation coefficient and the chi-square test.

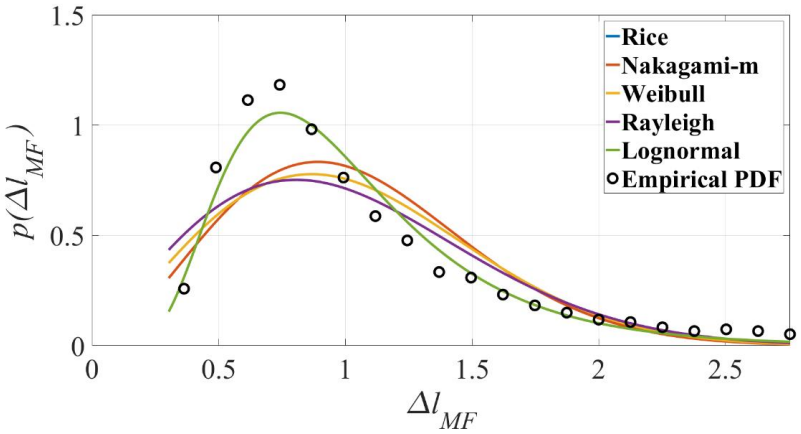

Figure 5. Exemplary results of the selected PDFs fitted to the empirical distribution of multipath fading (for DEP, AB_L, NB, and LOS).

To present the results in a tabular form, a unified description of the P_1 and P_2 distributions' parameters was used, where:

- for Rice distribution, P_1 is the non-centrality parameter s_R and P_2 is the scale parameter σ_R,
- for Nakagami-*m* distribution, P_1 is the shape parameter m and P_2 is the scale parameter Ω,
- for Weibull distribution, P_1 is the shape parameter α_W and P_2 is the scale parameter β_W,
- for Rayleigh distribution, P_1 is a scale parameter σ_{RAY}, and
- for lognormal distribution, P_1 is the mean value μ and P_2 is the standard deviation σ, both expressed in (dB).

Tables 3–5 show the detailed list of fitted distributions' parameters for different MN placements and scenarios. The threshold value of the chi-square test is the same as for the body shadowing case.

Table 3. The parameters of PDFs fitted to empirical distributions of small-scale fading amplitudes for HE_R.

MN	SCN	LOS/NLOS	PDF	868 MHz NB				6489 MHz UWB			
				P_1	P_2	χ^2	r	P_1	P_2	χ^2	r
HE_R	APR	LOS	Rice	0.036	0.831	13.72	0.90	0.934	0.298	5.78	0.86
			Nakagami-*m*	1.164	1.384	12.45	0.88	3.262	1.050	5.23	0.89
			Weibull	1.181	2.036	11.61	0.89	1.090	3.363	5.75	0.82
			Rayleigh	0.832	-	13.72	0.90	0.725	-	5.74	0.64
			Lognormal	**−0.081**	**0.484**	**10.66**	**0.97**	**−0.056**	**0.275**	**11.90**	**0.95**
		NLOS	Rice	0.814	0.523	7.70	0.91	0.923	0.400	10.11	0.94
			Nakagami-*m*	1.552	1.209	7.87	0.94	2.001	1.173	9.14	0.98
			Weibull	1.138	2.398	7.65	0.92	1.141	2.909	9.91	0.95
			Rayleigh	0.777	-	7.34	0.90	0.766	-	5.22	0.85
			Lognormal	**−0.083**	**0.423**	**7.64**	**0.99**	**−0.055**	**0.387**	**4.87**	**0.99**
	DEP	LOS	Rice	0.062	0.792	6.44	0.90	0.914	0.387	6.20	0.87
			Nakagami-*m*	1.410	1.258	11.32	0.91	2.149	1.136	5.59	0.91
			Weibull	1.150	2.252	8.04	0.90	1.124	2.885	6.03	0.87
			Rayleigh	0.793	-	6.43	0.90	0.754	-	5.38	0.80
			Lognormal	**−0.083**	**0.434**	**8.46**	**0.99**	**−0.061**	**0.354**	**4.76**	**0.98**
		NLOS	Rice	0.053	0.806	9.53	0.90	0.919	0.409	10.01	0.94
			Nakagami-*m*	1.286	1.301	11.73	0.89	1.939	1.179	9.06	0.98
			Weibull	1.160	2.152	10.75	0.89	1.142	2.871	9.83	0.95
			Rayleigh	0.807	-	9.52	0.90	0.768	-	7.17	0.87
			Lognormal	**−0.087**	**0.457**	**10.74**	**0.98**	**−0.058**	**0.395**	**6.67**	**0.99**

Table 4. The parameters of PDFs fitted to empirical distributions of small-scale fading amplitudes for TO_F.

MN	SCN	LOS/NLOS	PDF	868 MHz NB				6489 MHz UWB			
				P_1	P_2	χ^2	r	P_1	P_2	χ^2	r
TO_F	APR	LOS	Rice	0.934	0.369	8.18	0.91	0.945	0.167	10.30	0.87
			Nakagami-*m*	2.304	1.144	7.39	0.92	8.802	0.948	9.92	0.87
			Weibull	1.131	3.034	7.92	0.91	1.030	5.322	7.78	0.83
			Rayleigh	0.756	-	4.05	0.87	0.689	-	0.68	0.53
			Lognormal	**−0.049**	**0.347**	**4.44**	**0.92**	**−0.055**	**0.169**	**8.90**	**0.85**
		NLOS	Rice	0.686	0.617	9.38	0.87	0.948	0.325	5.27	0.96
			Nakagami-*m*	1.507	1.231	11.04	0.87	2.698	1.111	4.51	0.98
			Weibull	1.144	2.320	10.45	0.86	1.119	3.478	5.42	0.95
			Rayleigh	0.785	-	10.98	0.88	0.745	-	2.09	0.69
			Lognormal	**−0.080**	**0.412**	**11.48**	**0.97**	**−0.046**	**0.332**	**4.30**	**0.97**
	DEP	LOS	Rice	0.908	0.384	8.28	0.94	0.941	0.313	4.05	0.96
			Nakagami-*m*	2.140	1.119	7.55	0.97	2.889	1.082	3.47	0.98
			Weibull	1.115	2.874	7.85	0.94	1.105	3.481	4.20	0.95
			Rayleigh	0.748	-	4.25	0.83	0.736	-	3.14	0.73
			Lognormal	**−0.070**	**0.360**	**6.41**	**0.98**	**−0.052**	**0.312**	**5.49**	**0.99**
		NLOS	Rice	0.051	0.813	14.02	0.89	0.913	0.409	9.91	0.95
			Nakagami-*m*	1.204	1.323	12.87	0.88	1.940	1.169	9.00	0.98
			Weibull	1.161	2.082	12.11	0.88	1.137	2.849	9.70	0.96
			Rayleigh	0.813	-	14.01	0.89	0.765	-	5.11	0.88
			Lognormal	**−0.095**	**0.477**	**11.51**	**0.98**	**−0.062**	**0.392**	**9.27**	**0.99**

For the majority of NB cases, the correlation coefficients satisfy the acceptance criteria. The best results were obtained for the lognormal distribution, although, in some cases, Nakagami-*m* also gives acceptable results. It may be observed that lognormal distribution fulfills the acceptability criteria for both GoF tests, regardless of the analyzed case. For the lognormal distribution, a significantly higher correlation coefficient was obtained compared to the other distributions. Thus, considering the data in the linear scale, the short-term fading is best described by the lognormal distributed random variable.

Similarly, all distributions fitted to the empirical UWB channel data are within the range of the acceptability of the chi-square test. It was also noticed that the value of the correlation coefficient in a few cases is greater than the selected acceptability threshold and typically oscillates close to this critical value. Based on the presented results, it can be assumed that the best results for the UWB

channel were obtained for the lognormal and Nakagami-*m* distributions. However, it was decided to choose the lognormal distribution, which yields slightly better GoF test results. It is worth noting that, for the analyzed measurement scenarios, the Rice and Rayleigh distributions should not be used to describe the small-scale fading amplitude distribution, which confirms the conclusions from the research carried out so far [38].

Table 5. The parameters of PDFs fitted to empirical distributions of small-scale fading amplitudes for AB_L.

MN	SCN	LOS/NLOS	PDF	868 MHz NB				6489 MHz UWB			
				P_1	P_2	χ^2	r	P_1	P_2	χ^2	r
AB_L	APR	LOS	Rice	0.831	0.503	8.47	0.87	0.925	0.341	6.56	0.89
			Nakagami-*m*	1.640	1.196	8.71	0.90	2.611	1.088	5.98	0.92
			Weibull	1.135	2.441	8.34	0.88	1.106	3.117	6.19	0.87
			Rayleigh	0.773	-	8.14	0.89	0.738	-	4.70	0.75
			Lognormal	**−0.078**	**0.399**	**5.95**	**0.98**	**−0.060**	**0.313**	**4.21**	**0.98**
		NLOS	Rice	0.049	0.811	12.54	0.91	0.915	0.422	9.63	0.93
			Nakagami-*m*	1.277	1.317	15.15	0.91	1.879	1.194	8.76	0.97
			Weibull	1.166	2.146	13.89	0.91	1.148	2.797	9.41	0.95
			Rayleigh	0.811	-	12.54	0.91	0.773	-	7.44	0.87
			Lognormal	**−0.082**	**0.464**	**10.57**	**0.99**	**−0.056**	**0.400**	**9.05**	**0.99**
	DEP	LOS	Rice	0.815	0.510	13.59	0.87	0.917	0.378	4.20	0.87
			Nakagami-*m*	1.607	1.184	13.92	0.91	2.219	1.127	3.68	0.92
			Weibull	1.128	2.411	13.47	0.89	1.121	2.941	4.08	0.88
			Rayleigh	0.769	-	7.98	0.88	0.751	-	3.15	0.80
			Lognormal	**−0.087**	**0.405**	**8.98**	**0.97**	**−0.061**	**0.348**	**4.58**	**0.98**
		NLOS	Rice	0.040	0.840	13.59	0.90	0.911	0.428	14.22	0.91
			Nakagami-*m*	1.107	1.414	15.23	0.89	1.860	1.195	13.23	0.95
			Weibull	1.186	1.977	13.35	0.90	1.148	2.770	13.90	0.92
			Rayleigh	0.841		13.58	0.90	0.773		4.38	0.87
			Lognormal	**−0.084**	**0.498**	**12.86**	**0.99**	**−0.057**	**0.398**	**5.58**	**0.99**

6. Statistical Analysis of the System Loss Model

The developed propagation model, whose components are determined by Equations (2), (5), and (6), can be expressed as:

$$L_{SL(\mathrm{dB})} = \overline{L_S(d_0)_{(\mathrm{dB})}} + 10{\cdot}n{\cdot}\log_{10}\left(\frac{d_{[\mathrm{m}]}}{d_{0[\mathrm{m}]}}\right) + 10{\cdot}\log_{10}\left[\Lambda\left(\mu_{B(\mathrm{dB})}, \sigma_{B(\mathrm{dB})}\right)\right] + 20{\cdot}\log_{10}\left[\Lambda\left(\mu_{F(\mathrm{dB})}, \sigma_{F(\mathrm{dB})}\right)\right] \quad (7)$$

where:

- $\Lambda\left(\mu_{B(\mathrm{dB})}, \sigma_{B(\mathrm{dB})}\right)$ is a random variable with lognormal distribution, which represents the power of the large-scale fading, due to the body shadowing effect, where μ_B and σ_B are the mean value and standard deviation, respectively;
- $\Lambda\left(\mu_{F(\mathrm{dB})}, \sigma_{F(\mathrm{dB})}\right)$ is a random variable with lognormal distribution, which represents the amplitude of the small-scale fading, caused by the multipath effect, where μ_F and σ_F are the mean value and standard deviation, respectively.

In order to analyze the accuracy of the developed propagation model, two statistical evaluation measures were used, i.e., the SEE and the ME [32]. In this case, the SEE is a measure of the model accuracy, and the ME determines the degree of dispersion of empirical data around the model. For the better fitting model, the SEE value is lower and the ME value is closer to 0 dB. It should be also noted that the model is considered to be sufficiently accurate if the SEE value does not exceed 8 dB [3,39].

Due to the two random factors included in Equation (7), it was decided to calculate both ME and SEE from 10,000 model simulations. In Table 6, the statistical analysis of the accuracy of the developed model for all scenarios is presented.

Table 6. A statistical analysis of accuracy of the developed model for all measurement scenarios.

MN LOCATION	SCENARIO	LOS/NLOS Conditions	868 MHz NB		6489 MHz UWB	
			SEE (dB)	ME (dB)	SEE (dB)	ME (dB)
HE_R	APR	LOS	7.3	−1.0	4.9	−0.4
		NLOS	7.3	−1.1	6.1	−0.5
	DEP	LOS	6.6	−0.9	6.4	−0.6
		NLOS	7.0	−0.9	6.5	−0.7
TO_F	APR	LOS	6.0	−0.7	5.2	−0.3
		NLOS	6.6	−0.9	6.2	−0.6
	DEP	LOS	6.2	−0.9	5.3	−0.6
		NLOS	7.2	−1.0	6.8	−0.8
AB_L	APR	LOS	6.1	−0.9	6.1	−0.5
		NLOS	7.2	−1.0	7.0	−0.7
	DEP	LOS	6.7	−0.9	6.1	−0.6
		NLOS	7.2	−0.9	7.0	−0.7

Considering the NB channel, the SEE and the ME values are similar across different MN placements and scenarios. The ME values are negative and within the range of $[-1.1; -0.7]$ dB. The SEE values are less than 8 dB for all analyzed scenarios and are within the range of [6.1; 7.3] dB.

For the UWB channel, the ME values are negative and are in the range of $[-0.8; -0.3]$. This indicates a small overestimation of the system loss according to the model. The values of the SEE are less than 8 dB for all scenarios and are in the range of [4.9; 7.0] dB.

Based on the obtained results, it was found that the developed model accurately describes the distribution of the system loss for the NB and UWB channels, operating at 868 MHz and 6489 MHz, respectively.

In Table 7, the general parameters of the channel model described by Equation (7) for LOS/NLOS conditions are presented. It is possible to use a generalized model in which the given ranges can be reduced to a single parameter value, by calculating the mean of its limit values. More detailed parameters of the model, which depend on the MN placements and scenarios, are given in Tables 1–5.

Table 7. Generalized parameters of the system loss model for an off-body communication in the ferryboat environment.

Model Parameters for 868 MHz NB Channel						
	n	$\overline{L_S(d_0)}$	$\bar{}_B$ (dB)	σ_B (dB)	$\bar{}_F$ (dB)	σ_F (dB)
LOS	[0.16; 0.34]	[64.7; 75.9]	[−0.2; 0.0]	[0.8; 2.0]	[−0.4; −0.2]	[1.5; 2.1]
NLOS	[1.40; 3.80] [1]	[65.9; 76.2]	[−0.4; −0.2]	[1.5; 2.6]	−0.4	[1.8; 2.2]
Model Parameters for 6489 MHz UWB Channel						
	n	$\overline{L_S(d_0)}$	$\bar{}_B$ (dB)	σ_B (dB)	$\bar{}_F$ (dB)	σ_F(dB)
LOS	[0.13; 0.85]	[23.4; 28.9]	[−0.3; −0.17]	[1.3; 2.2]	[−0.3; −0.2]	[0.7; 1.5]
NLOS	[1.25; 3.46]	[26.1; 30.7]	[−0.3; −0.2]	[1.7; 2.8]	[−0.3; −0.2]	[1.4; 1.7]

[1] Excluding the HE_R scenario, where $n = 0.16$.

7. Conclusions

The growing demand for health monitoring devices, i.e., recording motion parameters or providing multimedia content, has contributed to the significant development of radio networks working within the human body or in its proximity. It applies directly to the evolution of WBANs, which is currently the major direction of modern 5G radio communication networks development, and (apart from medicine) are widely used in the entertainment, marketing, and security. To design

such systems, it is very important to have an accurate radio channel model, especially when they are supposed to work in harsh environments.

In the article, the off-body NB and UWB system loss model for WBANs in a ferryboat environment is described. A mobile heterogeneous measurement equipment, which consists of three devices: miniaturized MN, stationary RN, and a DAS, was developed. The time-synchronized RDMs, implemented in the UWB interface, are a novel approach to system loss measurements and they enable one to automatize the measurement process and simplify the data analysis. Dynamic scenarios corresponding to a typical human behavior in an indoor environment were considered, where the lack of direct antenna visibility conditions, due to the presence of structural elements of the environment, were distinguished.

A detailed analysis of both radio channels' parameters was carried out. An analysis of the system loss distributions, SLE, MSL, large-scale fading corresponding to body shadowing and small-scale fading associated with the multipath phenomenon both for the NB and UWB channels was performed. The obtained SLE values are in the range of [0.16; 3.8] for the NB channel, and [0.13; 3.46] for the UWB one. The lower values correspond to the LOS and the higher ones to the NLOS conditions. In addition, the MSL values at the reference distance for the NB channel, being in [64.7; 76.2], are much higher than in the UWB one, i.e., in [23.4; 30.7]. This is due to the transmission techniques, body influence, used antennas, and the impact of the environment.

The lognormal distribution is indicated as the best model for large- and small-scale fading, regardless of the MN placement. The large-scale fading mean value is in the range of $[-0.4; 0]$, and the standard deviation is in [0.8; 2.6] for the NB channel, while these ranges are, respectively, $[-0.3; -0.17]$ and [1.3; 2.8], for the UWB one. The small-scale fading distribution mean value in the range of $[-0.4; -0.2]$, standard deviation in [1.5; 2.2] for NB channel and, respectively, $[-0.3; -0.2]$ and [0.7; 1.7] for UWB channel, should be considered for radio link designing. A statistical analysis of the model parameters was also carried out and its good fit to the empirical data was demonstrated.

Future work will focus on determining the system loss model dependency on frequency. The behavior of channel impulse response, especially in the UWB channel, in accordance to the MN placement on the human body will be investigated.

Author Contributions: All authors contributed to developing the measurement equipment, designing and performing measurements, data analysis, scientific discussions, and writing the paper.

Acknowledgments: This work was developed within framework of the COST Action CA15104 "Inclusive Radio Communication Networks for 5G and beyond" (IRACON) and with financial support of the Faculty of Electronics, Telecommunications and Informatics of Gdansk University of Technology.

Conflicts of Interest: The authors declare no conflict of interest.

References

1. ETSI. *Universal Mobile Telecommunications System (UMTS); Evaluation of the Inclusion of Path Loss Based Location Technology in the UTRAN*; Technical Report TR 125 907, V9.0.1, 02/2010; ETSI: Sophia Antipolis, France, 2010.
2. Góra, J. 5G Technology Development—From Idea to Product. *Telecommunications Review and Telecommunications News*, No. 6/2017. (In Polish)
3. Lee, W.C.Y. *Mobile Cellular Telecommunications Systems*; McGraw-Hill: New York City, NY, USA, 1989.
4. Iguchi, T. Will Telepathy One Be Able to Change the World? Available online: www.medium.com (accessed on 14 June 2018).
5. Bednarczyk, W.; Gajewski, P.; Nowosielski, L. Energy-Efficient Dynamic Spectrum Management in Cognitive Radio Sensor Networks. In Proceedings of the 2016 Progress in Electromagnetic Research Symposium (PIERS), Shanghai, China, 8–11 August 2016.
6. Cardona, N. *Cooperative Radio Communications for Green Smart Environments*; River Publishers Series in Communications; River Publishers: Gistrup, Denmark, 2016.
7. Cavallari, R.; Martelli, F.; Rosini, R.; Buratti, C.; Verdone, R. A Survey on Wireless Body Area Networks: Technologies and Design Challenges. *IEEE Commun. Surv. Tutor.* **2014**, *16*, 1635–1657. [CrossRef]

8. European Commission. *COST Action 231, Digital Mobile Radio towards Future Generation Systems*; Final Report; European Commission: Luxemburg, 1999.
9. Maćkowiak, M.Ł. Modelling MIMO Systems in Body Area Networks in Outdoors. Ph.D. Thesis, Universidade Tecnica de Lisboa, Instituto Superior Tecnico, Lisboa, Portugal, 2013.
10. Oliveira, C. Characterisation of On-Body Communications. Ph.D. Thesis, Universidade Tecnica de Lisboa, Instituto Superior Tecnico, Lisboa, Portugal, 2013.
11. Sadowski, J.; Rajchowski, P.; Cwalina, K. Tracking Body Movement for Radio Channel Measurements in BAN with Indoor Positioning System. In Proceedings of the 2016 URSI Asia-Pacific Radio Science Conference (URSI AP-RASC), Seoul, Korea, 21–25 August 2016.
12. Kdouh, H.; Brousseau, C.; Zaharia, G.; Grunfelder, G.; El Zein, G. Measurements and Path Loss Models for Shipboard Environments at 2.4 GHz. In Proceedings of the 41st European Microwave Conference (EuMC), Manchester, UK, 10–13 October 2011.
13. Kumpuniemi, T.; Tuovinen, T.; Hämäläinen, M.; Yazdandoost, K.Y.; Vuohtoniemi, R.; Iinatti, J. Measurement-Based On-Body Path Loss Modelling for UWB WBAN Communications. In Proceedings of the 7th International Symposium on Medical Information and Communication Technology, Tokyo, Japan, 6–8 March 2013.
14. Zhai, S.; Jiang, T.; Li, D.; Li, B. Statistical Characterization of UWB Propagation Channel in Ship Cabin Environment. In Proceedings of the 2012 IEEE International Conference on Communications (ICC), Ottawa, ON, Canada, 10–15 June 2012.
15. Xia, L.; Redfield, S.; Chiang, P. Experimental Characterization of a UWB Channel for Body Area Networks. *EURASIP J. Wirel. Commun. Netw.* **2011**, *2011*, 703239. [CrossRef]
16. Kosz, P.T.; Ambroziak, S.J.; Stefanski, J.; Cwalina, K.K.; Correia, L.M.; Turbic, K. An Empirical System Loss Model for Body Area Networks in a Passenger Ferry Environment. In Proceedings of the Baltic URSI Symposium, Poznan, Poland, 14–17 May 2018.
17. AdeunisRF. *Narrowband NB868-500mW RF Module,* v.2.2.5; AdeunisRF: Crolles, France, 2014.
18. DecaWave, ScenSor, Designing the First Commercial IEEE 802.15.4a chip. In Proceedings of the IEEE 27th Convention of Electrical & Electronics Engineers in Israel, At Eilat, Israel, 14–17 November 2012.
19. *IEEE 802.15.6-2012, IEEE Standard for Local and Metropolitan Area Networks—Part 15.6: Wireless Body Area Networks*; IEEE: New York, NY, USA, 2012.
20. Datasheet. *Wireless Components FR4 Chip Antenna ANT1204F007R0870A UF (870 MHz), 1024 Series*; Yageo: Taipei, Taiwan, 2013.
21. Datasheet. *ACS5200HFAUWB Dielectric Chip Antenna*; Partron: Seoul, Korea, 2014.
22. Datasheet. *Getac F110 Fully Rugged Tablet*, Rugged Mobile Computing Solutions.
23. Latre, B.; Braem, B.; Moerman, I.; Blondia, C.; Demeester, P. A Survey on Wireless Body Area Networks. *Wirel. Netw.* **2011**, *17*, 1–18. [CrossRef]
24. Negra, R.; Jemili, I.; Belghith, A. Wireless Body Area Networks: Applications and Technologies. *Procedia Comput. Sci.* **2016**, *83*, 1274–1281. [CrossRef]
25. Ambroziak, S.J.; Correia, L.M.; Turbic, K. Radio Channel Measurements in Body-to-body Communications in Different Scenarios. In Proceedings of the 2016 URSI Asia-Pacific Radio Science Conference (URSI AP-RASC), Seoul, Korea, 21–25 August 2016.
26. DecaWave. *APS011 Application Note, Sources of Error in DW1000 Based Two-Way Ranging (TWR) Schemes*; DecaWave: Shenzhen, China, 2014.
27. Ambroziak, S.J.; Turbic, K.; Oliveira, C.; Correia, L.M.; Katulski, R.J. Fading Modelling in Dynamic Off-body Channels. In Proceedings of the 2016 10th European Conference on Antennas and Propagation (EuCAP), Davos, Switzerland, 10–15 April 2016.
28. Ambroziak, S.J.; Correia, L.M.; Katulski, R.J.; Mackowiak, M.; Oliveira, C.; Sadowski, J.; Turbic, K. An Off-Body Channel Model for Body Area Networks in Indoor Environments. *IEEE Trans. Antennas Propag.* **2016**, *64*, 4022–4035. [CrossRef]
29. Cwalina, K.K.; Ambroziak, S.J.; Rajchowski, P.; Correia, L.M. Radio Channel Measurements in 868 MHz Off-Body Communications in a Ferry Environment. In Proceedings of the 2017 XXXIInd General Assembly and Scientific Symposium of the International Union of Radio Science (URSI GASS), Montreal, QC, Canada, 19–26 August 2017.

30. Cwalina, K.K.; Ambroziak, S.J.; Rajchowski, P.; Correia, L.M. System Loss in UWB Off-Body Communications in a Ferry Environment. In Proceedings of the Baltic URSI Symposium, Poznan, Poland, 14–17 May 2018.
31. ITU–R P.341–6, The Concept of Transmission Loss for Radio Link. 2016. Available online: https://www.itu.int/rec/R-REC-P.341/en (accessed on 10 April 2018).
32. Ambroziak, S.J.; Katulski, R.J. An Empirical Propagation Model for Mobile Radio Links in Container Terminal Environment. *IEEE Trans. Veh. Technol.* **2013**, *62*, 4276–4287. [CrossRef]
33. Rappaport, T. *Wireless Communications: Principles and Practice*, 2nd ed.; Prentice Hall PTR: Upper Saddle River, NJ, USA, 2001.
34. Kaur, S.; Malhotra, J. Survey on Empirical Channel Models for WBAN. *Int. J. Future Gen. Commun. Netw.* **2015**, *8*, 399–410. [CrossRef]
35. Ghassemzadeh, S.S.; Greenstein, L.J.; Kavcic, A.; Sveinsson, T.; Tarokh, V. UWB Indoor Path Loss Model for Residential and Commercial Buildings. In Proceedings of the 2003 IEEE 58th Vehicular Technology Conference, Orlando, FL, USA, 6–9 October 2003.
36. Thotahewa, K.M.S.; Redoute, J.-M.; Yuce, M.R. *Ultra Wideband Wireless Body Area Networks*; Springer: Berlin, Germany, 2014.
37. Ginos, B.F. Parameter Estimation for the Lognormal Distribution. All Theses and Dissertations, Article no. 1928. 2009. Available online: https://scholarsarchive.byu.edu/etd/1928/ (accessed on 10 April 2018).
38. Smith, D.B.; Hanlen, L.W. *Channel Modeling for Wireless Body Area Networks*; Ultra-Low-Power Short-Range Radios, Integrated Circuits and Systems; Springer: Cham, Switzerland, 2015.
39. Rozal, E.O.; Palaes, E.G. Statistical Adjustment of Walfisch-Ikegami Model based in Urban Propagation Measurements. In Proceedings of the 2007 SBMO/IEEE MTT-S International Microwave and Optoelectronics Conference, Salvador, Brazil, 29 October–1 November 2007.